

STOP: Spatiotemporal Orthogonal Propagation for Weight-Threshold-Leakage Synergistic Training of Deep Spiking Neural Networks

Haoran Gao, *Student Member, IEEE*, Xichuan Zhou, *Senior Member, IEEE*, Yingcheng Lin, Min Tian, *Member, IEEE*, Liyuan Liu, *Member, IEEE* and Cong Shi*, *Member, IEEE*

Abstract—The prevailing of artificial intelligence-of-things calls for higher energy-efficient edge computing paradigms, such as neuromorphic agents leveraging brain-inspired spiking neural network (SNN) models based on spatiotemporally sparse binary activations. However, the lack of efficient and high-accuracy deep SNN learning algorithms prevents them from practical edge deployments with a strictly bounded cost. In this paper, we propose a spatiotemporal orthogonal propagation (STOP) algorithm to tackle this challenge. Our algorithm enables fully synergistic learning of synaptic weights as well as firing thresholds and leakage factors in spiking neurons to improve SNN accuracy, while under a unified temporally-forward trace-based framework to mitigate the huge memory requirement for storing neural states of all time-steps in the forward pass. Characteristically, the spatially-backward neuronal errors and temporally-forward traces propagate orthogonally to and independently of each other, substantially reducing computational overhead. Our STOP algorithm obtained high recognition accuracies of 99.53%, 94.84%, 74.92%, 98.26% and 77.10% on the MNIST, CIFAR-10, CIFAR-100, DVS-Gesture and DVS-CIFAR10 datasets with adequate SNNs of intermediate scales from LeNet-5 to ResNet-18. Compared with other deep SNN training works, our method is more plausible for edge intelligent scenarios where resources are limited but high-accuracy in-situ learning is desired.

Index Terms—neuromorphic computing, spiking neural network (SNN), backpropagation through time (BPTT), spatiotemporal backpropagation (STBP), synergistic learning

I. INTRODUCTION

Deep learning [1]-[3] have found a tremendous amount of applications across a widespread range of intelligent scenarios including assisted driving, security monitor,

This work was funded in part by the National Natural Science Foundation of China under Grant No. 62334008, in part by the Opening Fund of Artificial Intelligence Key Laboratory of Sichuan Province under Grant No. 2023RYY07, and in part by the by the Fundamental Research Funds for the Central Universities under Grant No. 2024CDJXY020.

Haoran Gao, Xichuan Zhou, Yingcheng Lin and Cong Shi are with the School of Microelectronics and Communication Engineering, Chongqing University, Chongqing 400044, China. (Corresponding author: Cong Shi, e-mail: shicong@cqu.edu.cn)

Min Tian is with Chongqing United Microelectronics Center Co. Ltd, Chongqing 401332, China.

Liyuan Liu is with the State Key Laboratory for Superlattices and Microstructures, Institute of Semiconductors, Chinese Academy of Sciences, Beijing 100083, China.

healthcare wearables, industrial robots, disaster prediction and so forth. However, conventional deep learning models relying on the continuously-valued artificial neural network (ANN) involve computationally intensive tensor multiplications. They are thus not suitable for ubiquitous edge devices in the era of artificial intelligence-of-things, where massive sensory data call for in-situ and adaptive processing under stringent energy, cost and latency budgets [4]. In contrast, the human brain is capable of conducting complex cognitive tasks while dissipating a bulb-level power as low as 20 W [5]. Such amazing energy efficiency arises in the mechanism of the cortical substrate that utilizes spatiotemporally sparse electric pulses (i.e., spikes) to exchange information among neurons. Inspired by this observation, the brain-mimicry spiking neural network (SNN) models [6] have emerged with substantially higher energy efficiency and lower computational latency than their ANN counterparts on dedicate neuromorphic silicon [7]-[17], expected to gain overwhelming popularity in versatile edge intelligent applications.

Early on, SNNs are primarily trained by the spike-timing dependent plasticity (STDP) rule [18], [19], which modifies synaptic weights of neurons according to their pre- and post-synaptic spike activities, optionally modulated by a global reward signal [20]. Despite its high biological plausibility and computational simplicity, the STDP rule usually results in limited recognition accuracies for SNNs compared with their ANN rivals whose weights are precisely adjusted via error gradient descent [21]. To bridge the performance gap between SNNs and ANNs, the ANN-SNN conversion method appears [22]-[28]. It treats the spike rate of a spiking neuron as an approximation of the continuous-valued activation of an artificial neuron. To obtain a high-accuracy SNN, a structurally equivalent ANN is first trained by the standard error backpropagation (BP) and gradient decent schemes, and then the learned weights are transferred to the SNN. However, such conversion method cannot leverage the precise timing of individual spikes and often calls for dozens to hundreds of time-steps to reach an acceptable level of activation approximation, which severely compromises SNN computation efficiency and incurs huge latencies on edge devices. Moreover, it is difficult and expensive to implement such conversion in an online manner for edge neuromorphic hardware processors. In recent years, BP-based techniques have been investigated for direct training of performant deep SNNs [29]-[30]. To overcome the non-continuity of spike activities, smooth surrogate gradients have been adopted to approximate the derivative of the non-differentiable spike firing function [31]. To handle the rich temporal dynamics in SNNs, the standard BP has to be extended

© 2024 IEEE. Personal use of this material is permitted. Permission from IEEE must be obtained for all other uses, in any current or future media, including reprinting/republishing this material for advertising or promotional purposes, creating new collective works, for resale or redistribution to servers or lists, or reuse of any copyrighted component of this work in other works. This work has been submitted to the IEEE for possible publication. Copyright may be transferred without notice, after which this version may no longer be accessible.

into the temporal dimension, and the errors need to propagate through both space (i.e., the layer depth) and time (i.e., the time-steps). The well-known backpropagation through time (BPTT) algorithm [32], originally proposed to train recurrent ANNs, can handle both explicit (due to recurrent synaptic weights) and implicit (due to inherent dynamics of spiking neurons) temporal dependencies in SNNs [33]. Considering the fact that many network topologies, especially those for the most common image classification tasks, do not necessarily contain recurrent synaptic connections, the BPTT algorithm reduces to the spatio-temporal backpropagation (STBP) rule for non-recurrent SNNs [34]. Compared to conversion-based methods, the BPTT and STBP algorithms can achieve comparable SNN accuracies yet with much fewer time-steps facilitating low-latency learning.

Nevertheless, the BPTT/STBP algorithms [32], [34] and their variants [35]-[38] bring forth a high memory cost for error BP. One has to store neural states (e.g., the internal membrane potential, the firing status, etc.) of all neurons across all time-steps in the feedforward pass, for later accesses during the backward pass [39]. Moreover, other model parameters like neural leakages and firing thresholds of individual spiking neurons need to be manually tuned, which imposes significant challenges on optimizing deep SNN accuracies.

Several techniques have emerged to alleviate the above disadvantages of the BPTT/STBP algorithms. One solution to lower the memory complexity is leveraging eligibility traces to delegate the temporal part of the error gradients with respect to synaptic weights [40]-[42]. Since the traces can be computed online in a forward manner along time-steps, the huge storage requirement for neuronal state backup no longer exists. During the backward pass, the output errors only need to backpropagate in the spatial domain. A more aggressive approach to mitigate memory-intensive temporal backpropagation is to completely ignore temporal dependencies between different time points [41], [43]-[45]. But this calls for other complicated mechanisms or poses specialized constraints on neural dynamics to maintain competent accuracies. To further improve SNN accuracy, a synergistic learning strategy is employed to concurrently train both synaptic weights and other key parameters (i.e., the firing thresholds [46]-[48] and the neural leakages [48]-[49]) under the STBP framework, acting as an alternative to the tedious manual parameter tuning process for accuracy improvement. However, these methods do not employ trace-based temporally forward propagation paradigm, thereby once again suffering the high memory complexity as in the original STBP algorithm.

This paper aims to achieve both high accuracy and high memory efficiency for non-recurrent deep SNN training. To this end, we propose the spatiotemporal orthogonal propagation (STOP) algorithm, which leverages a unified temporally-forward trace-based framework to implement fully weight-threshold-leakage (WTL) synergistic learning. The synaptic weights, the firing thresholds and the neural leakages all have their own traces, which are computed and forward propagated in the time, orthogonal to the spatial error backpropagation flow. In other words, the temporal traces and the spatial gradients are propagated independently of each other. On top of that, the high-accuracy algorithm does not necessarily exploit

sophisticated spiking neuron models [37], [40], [43], auxiliary decision/loss functions [42], [43], [44], [46], [47] or mandatory normalizations [34], [35], [36], [44], making it very attractive to edge systems with quite limited memory and computing resources. The main contributions of this article are two folds:

- We propose the STOP algorithm to enable high-accuracy and memory-efficient WTL synergistic learning of deep SNNs within a unified temporally-forward trace-based framework. To the best of our knowledge, this is the first time that firing thresholds and neural leakage factors are learned forwardly along the temporal axis.
- We have conducted extensive experiments to validate the efficacy of the proposed STOP algorithm on static image datasets: MNIST, CIFAR-10, CIFAR-100, as well as more challenging neuromorphic datasets: DVS-Gesture and DVS-CIFAR10, with various deep convolutional SNNs.

The rest of this paper is organized as follows. Section II describes the foundations including the spiking neuron model, input encoding, output decoding and the loss function adopted in our work. Section III presents the proposed STOP algorithm for memory-efficient training of deep feedforward SNNs. The high accuracy of our algorithm is validated in Section IV, along with related work comparisons and discussions. Section V concludes this paper and indicates future directions.

II. SNN PRELIMINARIES

A. Leaky Integrate-and-Fire Spiking Neuron

The most commonly used spiking neuron model in SNNs is the leaky integrate-and-fire (LIF) neuron characteristic of a good balance between biological plausibility and computational efficiency [6]. Fig. 1(a) shows a feedforward SNN composed of LIF neurons, whose model structure and temporal dynamics are illustrated in Fig. 1(b). The LIF spiking neuron continuously integrates weighted incoming (i.e., presynaptic) spikes onto its membrane potential via a set of synapses. Once its membrane potential crosses the firing threshold, the neuron issues an outgoing (i.e., postsynaptic) spike, and immediately resets itself by subtracting the threshold from the membrane potential. Meanwhile, the membrane potential is exponentially leaking all the time. More particularly, the temporal dynamics of an LIF neuron in the discrete time domain can be formulated as:

$$I_j^t[t] = \sum_i w_{ji}^t s_i^{t-1}[t] \quad (1a)$$

$$R_j^t[t] = U_j^t[t-1] - \theta_j^t s_j^t[t-1] \quad (1b)$$

$$U_j^t[t] = \alpha^t R_j^t[t] + I_j^t[t] \quad (1c)$$

$$F_j^t[t] = U_j^t[t] - \theta_j^t \quad (1d)$$

$$s_j^t[t] = H(F_j^t[t]) \quad (1e)$$

where t represents the discrete time-step, I_j^t , U_j^t , s_j^t , and $\theta_j^t > 0$ are the dendritic current, the membrane potential, the fired binary spike, and the firing threshold and the leakage factor of

© 2024 IEEE. Personal use of this material is permitted. Permission from IEEE must be obtained for all other uses, in any current or future media, including reprinting/republishing this material for advertising or promotional purposes, creating new collective works, for resale or redistribution to servers or lists, or reuse of any copyrighted component of this work in other works. This work has been submitted to the IEEE for possible publication. Copyright may be transferred without notice, after which this version may no longer be accessible.

neuron j in layer l , respectively, $0 \leq \alpha^l \leq 1$ is the leakage factor shared by all neurons in layer l , w_{ji}^l denotes the weight of the synapse connecting this neuron and a particular presynaptic neuron indexed as i in the preceding layer, and $H(x)$ is the firing action based on the Heavyside step function: $H(x) = 1$ or 0 when $x \geq 0$ or $x < 0$, respectively. R_j^l accounts for a reset operation, and F_j^l is employed as an intermediate variable.

From Eq. (1a) - (1e), we can easily deduce the following ones:

$$\frac{\partial U_j^l[t]}{\partial w_{ji}^l} = s_i^{l-1}[t] \quad (2)$$

$$\frac{\partial U_j^l[t]}{\partial s_i^{l-1}[t]} = \frac{\partial U_j^l[t]}{\partial s_i^{l-1}[t]} = w_{ji}^l \quad (3)$$

$$\frac{\partial F_j^l[t]}{\partial U_j^l[t]} = 1 \quad (4)$$

$$\frac{\partial s_j^l[t]}{\partial U_j^l[t]} = \frac{\partial s_j^l[t]}{\partial F_j^l[t]} = \varphi_{\text{SG}}(F_j^l[t]) = \varphi_{\text{SG}}(U_j^l[t] - \theta_j^l) \quad (5)$$

where $\varphi_{\text{SG}}(x)$ is a *surrogate gradient* function to approximate the derivative of non-differentiable spike firing function $H(x)$ in Eq. (1e). Some common forms of $\varphi_{\text{SG}}(x)$ are given in [34], and Fig. 2 gives two typical exemplars.

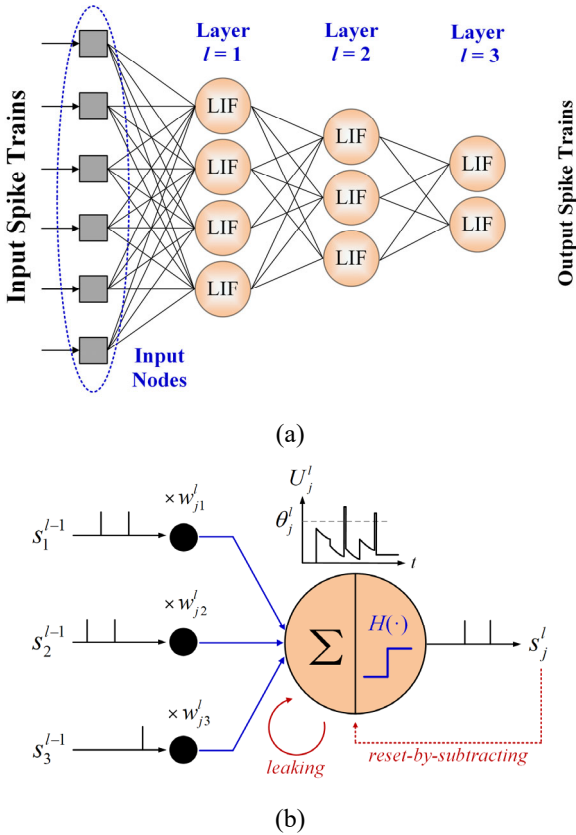


Fig. 1. (a) A feedforward SNN consisting of LIF neurons. (b) Temporal dynamics of LIF neuron.

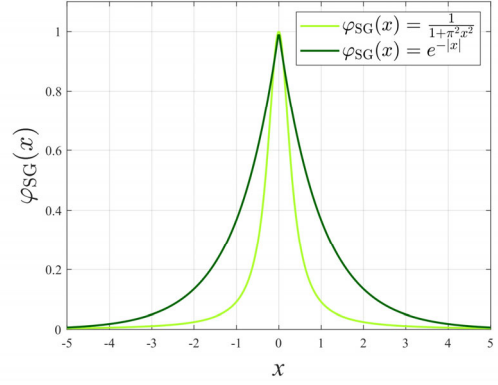


Fig. 2. Typical surrogate gradient functions [34].

B. Input Encoding

There are three mainstream methods for encoding continuous values (e.g., the pixel data in an image sample) before they are fed to SNNs. The rate coding method [50] converts a data value to a Poisson-distributed spike train at a rate proportional to the value, gaining robustness at higher computation overheads. The temporal coding method, on the contrary, transforms the value into a single spike occurring at a time inversely proportional to the value, trading off robustness for computational efficiency [50]. Recently, direct coding has dominated the regime of high-accuracy deep SNN training [36]. It rescales input values to the continuous range of $[0,1]$ and treats them as fractional spikes (in contrast to the ordinary binary spikes) repeatedly entering SNN at every time-step. In this work, we adopt the direct encoding.

C. Output Decoding

In an object classification task, each neuron in the output layer is uniquely pre-allocated to a particular object category. During inference, the neuron firing the most spikes indicates the classification result of the input sample.

D. Loss Function

The loss function reflects the deviations of actual SNN output spikes from desired outputs, and it is used to compute the errors of neurons for synaptic weight updates. The total loss E is the aggregation of instantaneous losses $E[t]$ across all time-steps. $E[t]$ usually takes the form of either mean squared error or cross-entropy (CE) loss, the latter of which behaves better in classification tasks and will be adopted in this work. Let the vector $\mathbf{s}^l[t] = (s_1^l[t], s_2^l[t], \dots)^T$ denote the actually fired spikes from neurons in the output layer $l = L$ at time t , and $\mathbf{s}^d = (s_1^d, s_2^d, \dots)^T$ the corresponding one-hot desired output spike vector (i.e., for each j , $s_j^d = 1$ if the category label of the training sample is j , and $s_j^d = 0$ otherwise), the CE loss $E[t]$ is defined as [36]:

$$E[t] = -\sum_j s_j^d \log(\text{softmax}(\mathbf{s}^l[t])_j) \quad (6)$$

where
$$\text{softmax}(\mathbf{s}^l[t])_j = \frac{\exp(s_j^l[t])}{\sum_k \exp(s_k^l[t])} \quad (7)$$

© 2024 IEEE. Personal use of this material is permitted. Permission from IEEE must be obtained for all other uses, in any current or future media, including reprinting/republishing this material for advertising or promotional purposes, creating new collective works, for resale or redistribution to servers or lists, or reuse of any copyrighted component of this work in other works. This work has been submitted to the IEEE for possible publication. Copyright may be transferred without notice, after which this version may no longer be accessible.

Based on the above loss function, we have:

$$\frac{\partial E[t]}{\partial s_j^l[t]} = \text{softmax}(\mathbf{s}^L[t])_j - s_j^d \quad (8)$$

III. THE PROPOSED STOP LEARNING ALGORITHM

In this section, we first describe trace-based learning rules for synaptic weights, firing thresholds and leakage factors in deep feedforward SNNs separately, and then combine them into our unified temporally-forward trace-based synergistic learning framework with precise forward and backward procedures.

A. Trace-based Weight Learning

Suppose one input training sample induces an output loss E . To apply the error to weight updates, we need to evaluate the derivative of the loss with respect to each synaptic weight:

$$\Delta w_{ji}^l = \frac{\partial E}{\partial w_{ji}^l} = \frac{\partial (\sum_t E[t])}{\partial w_{ji}^l} = \sum_t \frac{\partial E[t]}{\partial w_{ji}^l} = \sum_t \frac{\partial E[t]}{\partial U_j^l[t]} \frac{\partial U_j^l[t]}{\partial w_{ji}^l} \quad (9)$$

Here we define:

$$\delta_j^l[t] = \frac{\partial E[t]}{\partial U_j^l[t]} \quad (10)$$

and

$$\tilde{w}_{ji}^l[t] = \frac{\partial U_j^l[t]}{\partial w_{ji}^l} \quad (11)$$

so that Eq. (9) can be re-written in a compact form as:

$$\Delta w_{ji}^l = \sum_t \delta_j^l[t] \tilde{w}_{ji}^l[t] \quad (12)$$

Here, $\delta_j^l[t]$ denotes the instantaneous derivative of the output loss at time t with respect to that neuron's membrane potential at the same time-step. It is called the error, or spatial gradient, of neuron j in layer l at time t . We solve $\delta_j^l[t]$ for all neurons via a spatial back-propagation procedure. For the output layer $l = L$, by taking into account Eq. (8) and (5), we obtain:

$$\begin{aligned} \delta_j^L[t] &= \frac{\partial E[t]}{\partial U_j^L[t]} = \frac{\partial E[t]}{\partial s_j^L[t]} \frac{\partial s_j^L[t]}{\partial U_j^L[t]} \\ &= (\text{softmax}(\mathbf{s}^L[t])_j - s_j^d) \varphi_{\text{sg}}(U_j^L[t] - \theta_j^L) \end{aligned} \quad (13)$$

Once the errors $\delta_j^{l+1}[t]$ of all neurons in layer $l+1$ have already been obtained, they can be spatially backpropagated to the lower layer l to compute the errors $\delta_j^l[t]$ via Eq. (3) and (5):

$$\begin{aligned} \delta_j^l[t] &= \frac{\partial E[t]}{\partial U_j^l[t]} = \sum_k \frac{\partial E[t]}{\partial U_k^{l+1}[t]} \frac{\partial U_k^{l+1}[t]}{\partial s_j^l[t]} \frac{\partial s_j^l[t]}{\partial U_j^l[t]} \\ &= \sum_k \delta_k^{l+1}[t] \frac{\partial U_k^{l+1}[t]}{\partial s_j^l[t]} \frac{\partial s_j^l[t]}{\partial U_j^l[t]} \\ &= (\sum_k \delta_k^{l+1}[t] w_{kj}^{l+1}) \varphi_{\text{sg}}(U_j^l[t] - \theta_j^l) \end{aligned} \quad (14)$$

This way, at each time-step t , the neuron errors $\delta_j^l[t]$ are layer-wisely backpropagated in the spatial domain.

On the other side, the $\tilde{w}_{ji}^l[t]$ defined in Eq. (11) represents the derivative of the neuron's membrane potential with respect to its weight, temporally accumulated up to time t . Actually, it can be computed efficiently in temporally-forward iterations. To achieve this, we differentiate both sides of Eq. (1c) with respect to w_{ji}^l and take into considerations Eq. (1b), (2) and (5), giving:

$$\begin{aligned} \frac{\partial U_j^l[t]}{\partial w_{ji}^l} &= \alpha^l \frac{\partial R_j^l[t]}{\partial w_{ji}^l} + \frac{\partial I_j^l[t]}{\partial w_{ji}^l} \\ &= \alpha^l \left(\frac{\partial U_j^l[t-1]}{\partial w_{ji}^l} - \theta_j^l \frac{\partial s_j^l[t-1]}{\partial U_j^l[t-1]} \frac{\partial U_j^l[t-1]}{\partial w_{ji}^l} \right) + s_i^{l-1}[t] \\ &= \alpha^l \frac{\partial U_j^l[t-1]}{\partial w_{ji}^l} - \alpha^l \theta_j^l \varphi_{\text{sg}}(U_j^l[t-1] - \theta_j^l) \frac{\partial U_j^l[t-1]}{\partial w_{ji}^l} + s_i^{l-1}[t] \end{aligned} \quad (15)$$

Substituting the $\tilde{w}_{ji}^l[t]$ definition in Eq. (11) into (15) leads to:

$$\tilde{w}_{ji}^l[t] = \alpha^l \tilde{w}_{ji}^l[t-1] - \underbrace{\alpha^l \theta_j^l \varphi_{\text{sg}}(U_j^l[t-1] - \theta_j^l) \tilde{w}_{ji}^l[t-1]}_{\text{illusory component}} + s_i^{l-1}[t] \quad (16)$$

which indicates that $\tilde{w}_{ji}^l[t]$ can be forwardly propagated in the temporal domain. However, it is noteworthy that the existence of the illusory component labeled in the above Eq. (16) relies on a surrogate gradient $\varphi_{\text{sg}}(x)$ that implies an *illusory fractional spike* with a value in between 0 and 1 to have always been fired at the previous time-step, as the smooth surrogate curves in Fig. 2 do not quickly drop to zero when $x < 0$. Therefore, such implicit existence of the illusory component appears to be unreasonable and it greatly complicates computations. Indeed, as will be discussed later in Section IV, temporal propagation of the illusory component performs often ineffectively or even occasionally detrimentally to SNN accuracy improvement. As a consequence, we preclude the illusory component from the temporal propagation, and Eq. (16) reduces to:

$$\tilde{w}_{ji}^l[t] = \alpha^l \tilde{w}_{ji}^l[t-1] + s_i^{l-1}[t] \quad (17)$$

Indeed, the temporally-forward spike-driven variable $\tilde{w}_{ji}^l[t]$ just plays the role of an eligibility trace [40]. It is confirmed that in the biological brain cortex, various traces serve as certain types of memorizations allowing for retention of temporally past events, and the traces can tell the impacts of those events on future neural system states [40]. Obviously, this trace initializes to $\tilde{w}_{ji}^l[0] = 0$, since $U_j^l[t] = 0$ whenever $t \leq 0$. Moreover, notice that the update of $\tilde{w}_{ji}^l[t]$ in Eq. (17) is only driven by spikes from corresponding neuron i in the preceding layer $l-1$ and is independent of the neuron index j in layer l . This suggests that we only need to track one trace for each neuron i of layer $l-1$, and share it with all neurons j in layer l .

Short summary for weight learning: Eq. (12) - (14) and (17) constitute the trace-based synaptic weight learning rule. For an input training sample, at each time-step $t = 1, 2, \dots, T$, the neuron errors (spatial gradients) $\delta_j^l[t]$ are spatially backpropagated from output layer $l = L$ down to the first layer $l = 1$ according to Eq. (13), (14), while the weight-related traces (temporal gradients) $\tilde{w}_{ji}^l[t]$ are temporally forward-propagated from time-step $t-1$ to t via Eq. (17). After the training sample presentation is over,

© 2024 IEEE. Personal use of this material is permitted. Permission from IEEE must be obtained for all other uses, in any current or future media, including reprinting/republishing this material for advertising or promotional purposes, creating new collective works, for resale or redistribution to servers or lists, or reuse of any copyrighted component of this work in other works. This work has been submitted to the IEEE for possible publication. Copyright may be transferred without notice, after which this version may no longer be accessible.

each weight is updated following Eq. (12). Section III-D will describe this procedure more formally with pseudocodes.

B. Trace-based Threshold Learning

Like synaptic weights, the firing thresholds of neurons can also be learned based on some temporally forward-propagated traces. Similar to Eq. (9), threshold updates are guided by the following gradient of the output loss with regard to thresholds:

$$\begin{aligned}\Delta\theta_j^l &= \frac{\partial E}{\partial \theta_j^l} = \sum_{\tau} \frac{\partial E[\tau]}{\partial \theta_j^l} = \sum_{\tau} \frac{\partial E[\tau]}{\partial F_j^l[\tau]} \frac{\partial F_j^l[\tau]}{\partial \theta_j^l} \\ &= \sum_{\tau} \frac{\partial E[\tau]}{\partial F_j^l[\tau]} \left(\frac{\partial F_j^l[\tau]}{\partial U_j^l[\tau]} \frac{\partial U_j^l[\tau]}{\partial \theta_j^l} - 1 \right)\end{aligned}\quad (18)$$

From Eq. (4), obviously the following relationship holds:

$$\frac{\partial E[\tau]}{\partial U_j^l[\tau]} = \frac{\partial E[\tau]}{\partial F_j^l[\tau]} \frac{\partial F_j^l[\tau]}{\partial U_j^l[\tau]} = \frac{\partial E[\tau]}{\partial F_j^l[\tau]}\quad (19)$$

By substituting Eq. (19) and (4) into Eq. (18), we attain:

$$\Delta\theta_j^l = \sum_{\tau} \frac{\partial E[\tau]}{\partial U_j^l[\tau]} \left(\frac{\partial U_j^l[\tau]}{\partial \theta_j^l} - 1 \right)\quad (20)$$

Inspired by Eq. (11), we likewise define:

$$\tilde{\theta}_j^l[\tau] = \frac{\partial U_j^l[\tau]}{\partial \theta_j^l}\quad (21)$$

By combining Eq. (20), (21) and (10), we have:

$$\Delta\theta_j^l = \sum_{\tau} \delta_j^l[\tau] (\tilde{\theta}_j^l[\tau] - 1)\quad (22)$$

Now, we differentiate both sides of Eq. (1c) with respect to θ_j^l . Since $I_j^l[\tau]$ in Eq. (1) is irrespective of θ_j^l and any illusory component evoked by the surrogate gradient, similar to that as analyzed in Eq. (16), should be dropped, we eventually have:

$$\frac{\partial U_j^l[\tau]}{\partial \theta_j^l} = \alpha^l \frac{\partial R_j^l[\tau]}{\partial \theta_j^l} + \frac{\partial I_j^l[\tau]}{\partial \theta_j^l} = \alpha^l \frac{\partial R_j^l[\tau]}{\partial \theta_j^l} = \alpha^l \left(\frac{\partial U_j^l[\tau-1]}{\partial \theta_j^l} - s_j^l[\tau-1] \right)\quad (23)$$

Substituting the $\tilde{\theta}_j^l[\tau]$ definition in Eq. (21) into (23) results in:

$$\tilde{\theta}_j^l[\tau] = \alpha^l (\tilde{\theta}_j^l[\tau-1] - s_j^l[\tau-1])\quad (24)$$

This indicates that $\tilde{\theta}_j^l[\tau]$ also acts as a trace that can be computed online in a temporally-forward manner as $\tilde{w}_{ji}^l[\tau]$ does in Eq. (17), expect the update of $\tilde{\theta}_j^l[\tau]$ is driven by postsynaptic spikes of the corresponding neuron and decays with the leakage factor of the neuronal membrane potential. Its initial values is $\tilde{\theta}_j^l[0] = 0$, too.

Short summary for threshold learning: Eq. (22), (13), (14) and (24) constitute the trace-based firing threshold learning rule. And the steps for threshold updates resemble the summary for weight learning in the previous subsection. Section III-D will leverage pseudocodes to describe these steps more precisely. Besides, the thresholds have to be truncated above 0 to satisfy the non-negative constraint each time they execute updates.

C. Trace-based Leakage Learning

Although the leakage factor is shared by all neurons in one layer, its update amount has to be evaluated over individual neurons and then averaged. To obtain each neuron's leakage factor change amount $\Delta\alpha_j^l$ via a temporally-forwarded trace, we first give the relevant output loss gradient:

$$\Delta\alpha_j^l = \sum_{\tau=1}^T \frac{\partial E[\tau]}{\partial \alpha^l} = \sum_{\tau=1}^T \frac{\partial E[\tau]}{\partial U_j^l[\tau]} \frac{\partial U_j^l[\tau]}{\partial \alpha^l}\quad (25)$$

Then, we define:

$$\tilde{\alpha}_j^l[\tau] = \frac{\partial U_j^l[\tau]}{\partial \alpha^l}\quad (26)$$

so that Eq. (25) becomes as:

$$\Delta\alpha_j^l = \sum_{\tau=1}^T \delta_j^l[\tau] \tilde{\alpha}_j^l[\tau]\quad (27)$$

Next, we differentiate both sides of Eq. (1c) with respect to α^l . Considering that $I_j^l[\tau]$ is irrelevant of α^l and that any illusory component originated from the surrogate gradient should not be preserved, we get:

$$\frac{\partial U_j^l[\tau]}{\partial \alpha^l} = \alpha^l \frac{\partial R_j^l[\tau]}{\partial \alpha^l} + \frac{\partial I_j^l[\tau]}{\partial \alpha^l} = \alpha^l \frac{\partial U_j^l[\tau-1]}{\partial \alpha^l} + R_j^l[\tau]\quad (28)$$

Substitute the $\tilde{\alpha}_j^l[\tau]$ definition in Eq. (26) into (28), and we have:

$$\tilde{\alpha}_j^l[\tau] = \alpha^l \tilde{\alpha}_j^l[\tau-1] + R_j^l[\tau]\quad (29)$$

which reveals that $\tilde{\alpha}_j^l[\tau]$ also functions as a trace characteristic of an online evaluation forwarded in the temporal domain. It is driven by the reset item in Eq. (1b) of the corresponding neuron and decays with the leakage factor, starting from $\tilde{\alpha}_j^l[0] = 0$.

Short summary for leakage learning: Eq. (27), (13), (14) and (29) constitute the trace-based leakage learning rule. Its detailed steps along with weight and threshold updates will be described soon in the next subsection. Remember that the updated leakage factors need to be truncated back to be within the range [0, 1].

D. Unified Trace-based STOP Synergistic Learning

We now combine the above trace-based learning of synaptic weights, firing thresholds and leakage factors into our unified memory-efficient temporally-forward trace-based synergistic learning framework for deep feedforward SNNs, wherein the spatial neuron errors can be reused for updates of all the three types of parameters. To learn one sample, at each time-step $t = 1, 2, \dots, T$ during the forward pass, the membrane potentials $U_j^l[t]$, as well as the weight-, threshold-, and leakage-related traces $\tilde{w}_{ji}^l[t]$, $\tilde{\theta}_j^l[t]$, and $\tilde{\alpha}_j^l[t]$ of all neurons are computed according to Eq. (1), (17), (24), (29), respectively, in a layer-wise fashion from $l = 1$ to $l = L$. And the instantaneous loss $E[t]$ is calculated via Eq. (6), (7) thereafter. Then, such loss is spatially backpropagated through all layers down to $l = 1$, to evaluate the neuron errors $\delta_j^l[t]$ by Eq. (13), (14). Next, for each neuron, the products of its error $\delta_j^l[t]$ and corresponding traces

© 2024 IEEE. Personal use of this material is permitted. Permission from IEEE must be obtained for all other uses, in any current or future media, including reprinting/republishing this material for advertising or promotional purposes, creating new collective works, for resale or redistribution to servers or lists, or reuse of any copyrighted component of this work in other works. This work has been submitted to the IEEE for possible publication. Copyright may be transferred without notice, after which this version may no longer be accessible.

Algorithm 1 STOP: temporally-forward trace-based weight-threshold-leakage synergistic learning for deep SNNs

Input: $s_i^0[t]$ — sample-encoded input spike trains;
 s_j^d — one-hot desired spike data for output neurons.
Parameter: T — total number of time-steps;
 L — SNN layer depth;
 N_l — number of neurons in layer l ;
 $\eta_w, \eta_\theta, \eta_\alpha$ — learning rates.
Output: w_{ji}^l — updated synaptic weights;
 θ_j^l — updated firing thresholds;
 α^l — updated leakage factors.

```

1: Initialize all variables  $U_j^l[0], \tilde{w}_{ji}^l[0], \theta_j^l[0]$  and  $\tilde{\alpha}^l[0]$  to 0;
2: for  $t = 1$  to  $T$  do
3:   // Spatial forward
4:   for  $l = 1$  to  $L$  do
5:     for  $j = 1$  to  $N_l$  do
6:       Compute  $U_j^l[t]$  by Eq. (1a) - (1c);
7:       Compute  $s_j^l[t]$  by Eq. (1d) - (1e);
8:       for  $i = 1$  to  $N_{l-1}$  do
9:         Compute  $\tilde{w}_{ji}^l[t]$  by Eq. (17);
10:      end for
11:      Compute  $\theta_j^l[t]$  by Eq. (24);
12:      Compute  $\tilde{\alpha}^l[t]$  by Eq. (29);
13:    end for
14:  end for
15:  // Spatial backward
16:  for  $l = L$  to  $1$  do
17:    for  $j = 1$  to  $N_l$  do
18:      if  $l = L$  then
19:        Compute loss  $E[t]$  in Eq. (6) using  $s_j^l[t], s_j^d$ ;
20:        Compute  $\delta_j^l[t]$  by Eq. (13);
21:      else
22:        Compute  $\delta_j^l[t]$  by Eq. (14);
23:      endif
24:      accumulate  $\delta_j^l[t]\tilde{w}_{ji}^l[t]$  to  $\Delta w_{ji}^l$  in Eq. (12);
25:      accumulate  $\delta_j^l[t](\theta_j^l[t] - 1)$  to  $\Delta\theta_j^l$  in Eq. (22);
26:      accumulate  $\delta_j^l[t]\tilde{\alpha}^l[t]$  to  $\Delta\alpha^l$  in Eq. (27);
27:    end for
28:  end for
29: end for
30: // Layer-wisely averaged changes for leakage factors
31: for  $l = 1$  to  $L$  do
32:    $\Delta\alpha^l \leftarrow \sum_i \alpha_i^l / N_i$ ;
33: end for
34: // Parameter updates
35: for  $l = 1$  to  $L$  do
36:   for  $j = 1$  to  $N_l$  do
37:     Update weight:  $w_{ji}^l \leftarrow w_{ji}^l - \eta_w \Delta w_{ji}^l$ ;
38:     Update threshold:  $\theta_j^l \leftarrow \max(0, \theta_j^l - \eta_\theta \Delta\theta_j^l)$ ;
39:   end for
40:   Update leakage:  $\alpha^l \leftarrow \max(0, \min(1, \alpha^l - \eta_\alpha \Delta\alpha^l))$ ;
41: end for

```

$\tilde{w}_{ji}^l[t], \theta_j^l[t]$, and $\tilde{\alpha}^l[t]$ at time t , i.e., $\delta_j^l[t]\tilde{w}_{ji}^l[t], \delta_j^l[t](\theta_j^l[t] - 1)$ and $\delta_j^l[t]\tilde{\alpha}^l[t]$, are accumulated to their corresponding change amounts $\Delta w_{ji}^l, \Delta\theta_j^l$ and $\Delta\alpha^l$, respectively. Finally, when all time-

steps of the training sample are over, these change amounts are scaled by their respective learning rates η_w, η_θ and η_α before they are applied to adjusting the corresponding parameters. In this learning procedure, we neither resort to temporally backward computing nor necessitate memorizing all neural states of every time-step across the forward pass, which is memory-costly as in the original BPTT and STBP algorithms. A more precise description of the above trace-based synergistic learning details on one training sample is given in Algorithm 1. Note that the update amounts of leakage factors are layer-wisely averaged as all neurons in one layer share the same leakage attribute. Moreover, if convolutional layers are involved, the update amounts of firing thresholds of neurons in each channel should further be averaged if the same firing threshold is adopted by all neurons in one channel [46]. Besides, the updated thresholds have to be truncated above 0 and the updated leakage factors need to be truncated within the range [0, 1], as mentioned in previous subsections.

Fig. 3 illustrates the error/gradient propagation flows in the proposed SNN training algorithm with totally $L = 4$ layers and $T = 4$ time-steps unrolled along the temporal axis. Note that for clarity, we only exhibit one neuron at each layer. As can be seen, the temporal gradients, i.e., the weight-, threshold- and leakage-related traces, are propagated forwardly in the temporal domain, while the spatial gradients, i.e., neuron errors, are propagated backwardly in the spatial domain. Although the two types of gradients must cooperate at each neuron node to accomplish parameter updates via Eq. (12), (22), (27), they are actually flowing independently of each other without fusion, so that temporal traces never carry information of spatial errors during their propagation, and vice versa. In other words, the spatial and temporal gradients are propagated in orthogonal pathways. This is why our algorithm is called *Spatiotemporal Orthogonal Propagation (STOP)*. Such paradigm not only saves substantial memory resources thanks to the employment of temporally forward traces, but also greatly simplifies computational graphs compared with the STBP algorithm [34], which has to re-merge the error gradients backward propagated along both spatial and temporal dimensions at every neuron and every time-step.

E. Complexity Analysis

TABLE I further compares the memory and computation complexities of the STBP [34] and our STOP algorithms, where STOP-W refers to the non-synergistic version of the STOP rule that only trains weights while STOP-WTL refers to the fully synergistic STOP rule that trains weights as well as thresholds and leakages. Without loss of generality, we assume a total of L layers in a fully-connected (FC) SNN, N neurons per layer on average and a sample presentation window of T time-steps long. Since the inference process always keeps the same regardless of particular learning rule, we only count in the extra memory and compute overheads needed for learning. Further, we merely consider multiplications as computation overheads and ignores other simple operations like additions, as these multiplications would consume much more power on edge systems.

© 2024 IEEE. Personal use of this material is permitted. Permission from IEEE must be obtained for all other uses, in any current or future media, including reprinting/republishing this material for advertising or promotional purposes, creating new collective works, for resale or redistribution to servers or lists, or reuse of any copyrighted component of this work in other works. This work has been submitted to the IEEE for possible publication. Copyright may be transferred without notice, after which this version may no longer be accessible.

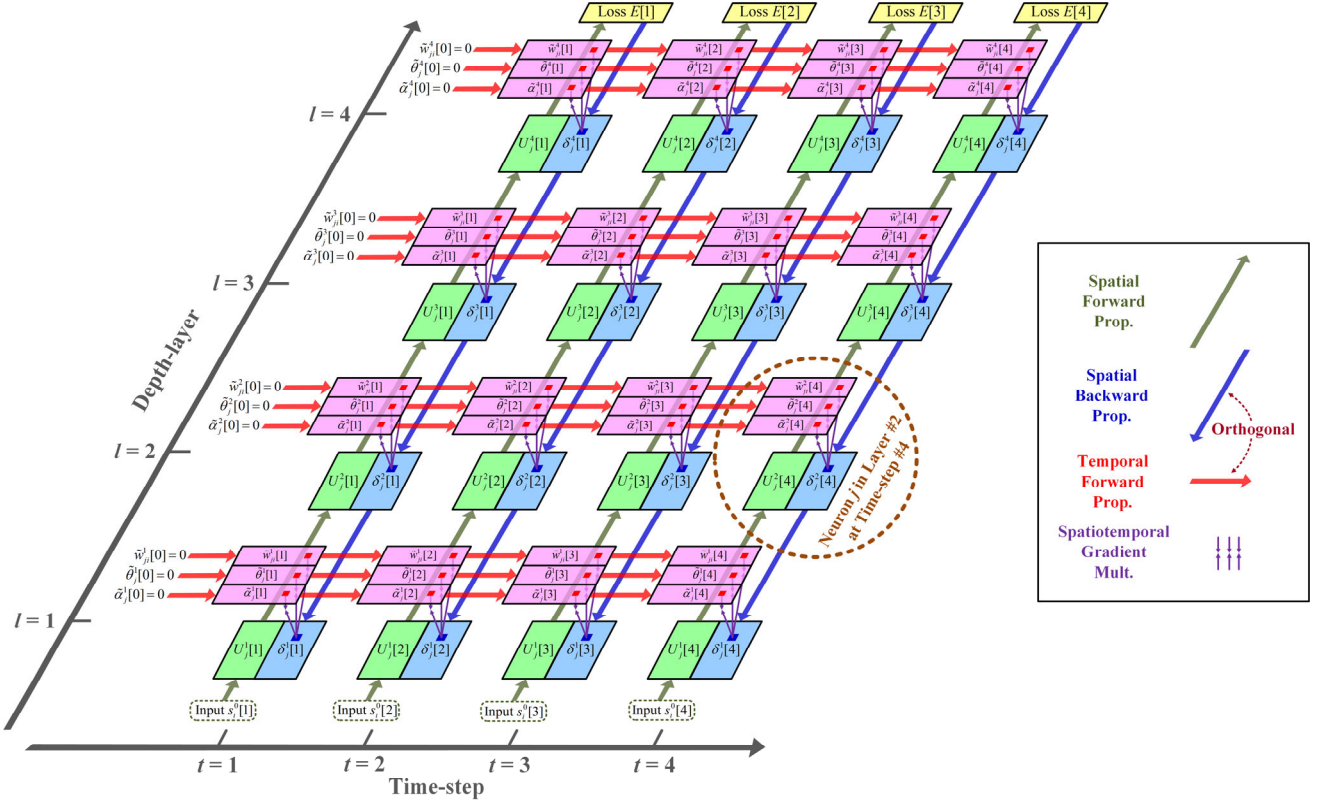


Fig. 3. Orthogonal propagation of spatially backward errors and temporally forward gradients.

a) *STBP*: As STBP requires backpropagating error gradients along both spatial and temporal dimensions, it has to store two neural state variables, i.e., the membrane potential and fired spike, of every neuron at every time-step during the forward pass for inquiry during the backward pass. Thus, its memory overhead or complexity is $O(2 \times N \times L \times T) = O(2NLT)$. Based on the spatiotemporal backpropagation calculation details given in Eq. (18) and (20) in [34], the STBP algorithm calls for $(N+7)$ multiplications to obtain the error of one neuron at a particular time-step from its downstream higher-layer neurons of the same time-step as well as from the neuron itself of the next time-step, and another N multiplications to calculate the updates of its N fan-in synaptic weights at that time-step. Hence, the whole SNN requires $O((N+7+N) \times N \times L \times T) = O((2N+7)NLT)$ multiplications throughout all T time-steps for one training sample.

b) *STOP-W*: Using temporally forward traces, the STOP-W rule has to store the membrane potential, fired spike and the weight-related traces of the neurons only for spatially backward error propagation at current time-step, which are then dropped at the next time-step. As explained above in Section III-A, such traces are shared by the neurons in one layer, and the number of traces for a layer equals to the count of neurons in its preceding layer. Since we have assumed that each layer holds N neurons on average, there is one such trace per neuron. Therefore, the memory complexity for the whole SNN is $O(3 \times N \times L) = O(3NL)$. The memory complexity ratio between STBP and STOP-W is $2NLT / 3NL = 2T/3$. In recent researches, T usually falls in the range from 6 to 10 [44], [48], so STOP-W outperforms STBP

by at least 4 times in terms of memory reduction. On the other side, for every neuron at each single time-step t , STOP-W requires $(N+1)$ multiplications to calculate the neuron's spatial error via Eq. (14), 1 multiplication to update the corresponding trace (to be shared by its downstream neurons in the subsequent layer) according to Eq. (17), as well as N multiplications to obtain the update amounts of the neuron's N synaptic weights for time t , as indicated by Eq. (12). Therefore, the STOP-W computation complexity for the whole SNN with NL neurons throughout all T times-steps is $O((N+1+1+N) \times N \times L \times T) = O((2N+2)NLT)$, which is approximate to that of STBP, as $(2N+7)NLT / (2N+2)NLT = (2N+7) / (2N+2) \approx 1$ considering that N is usually at the order of hundreds or even thousands. Although it implies that STOP-W and STBP has similar computation complexities, the orthogonal graph of independent spatial and temporal gradient propagations in the STOP-W rule would facilitate cost-efficient hardware circuit design if customized neuromorphic processor is demanded.

c) *STOP-WTL*: On top of STOP-W, the fully synergistic learning rule STOP-WTL needs additional memory space for one threshold-trace and one leakage-related trace per neuron. As a result, its total memory complexity is $O(5 \times N \times L) = O(5NL)$, which is still $\times 1.2 \sim \times 2$ less than the STBP algorithm that only allows to train synaptic weights, when T varies between 6 and 10 as mentioned above. Likewise, for each neuron, due to the additional 4 multiplications for tracking the threshold- and leakage-related traces in Eq. (24), (29) as well as computing the update amounts of firing thresholds and leakage factors at every

© 2024 IEEE. Personal use of this material is permitted. Permission from IEEE must be obtained for all other uses, in any current or future media, including reprinting/republishing this material for advertising or promotional purposes, creating new collective works, for resale or redistribution to servers or lists, or reuse of any copyrighted component of this work in other works. This work has been submitted to the IEEE for possible publication. Copyright may be transferred without notice, after which this version may no longer be accessible.

time-step t in Eq. (22), (27), the computation complexity slightly rises to $O((N+1+1+N+4) \times N \times L \times T) = O((2N+6)NLT)$. This is almost the same as that of STBP, but our STOP rule can achieve fully synergistic learning towards higher SNN accuracy, and is more cost-effective for edge hardware implementation as analyzed just soon.

TABLE I

MEMORY AND COMPUTATION OVERHEADS IN DIFFERENT SNN LEARNING RULES

Method	Memory complexity	Computation complexity
STBP [34]	$O(2TLN)$	$O(TLN(2N+7))$
STOP-W	$O(3LN)$	$O(TLN(2N+2))$
STOP-WTL	$O(5LN)$	$O(TLN(2N+6))$

Note: L — layer depth, N — average number of neurons per layer, T — number of time-steps for one sample presentation

IV. EXPERIMENTAL RESULTS

A. Experimental Setup

In this section, we evaluated the proposed STOP algorithm on both static image datasets (MNIST [21], CIFAR-10 [51], CIFAR-100 [51]) and neuromorphic visual datasets (DVS-Gesture [52] and DVS-CIFAR10 [53]) with adequate small- to mediate-scale deep SNN architectures, as listed in TABLE II. For instance, Lenet-5 was deemed to be sufficient for high-accuracy learning on the MNIST dataset [34], while deeper VGG-11 or Resnet-18 networks guaranteed accuracy performance on more challenging benchmarks like CIFAR-10/100. As SNNs and our algorithm primarily target on edge intelligence, much larger datasets like ImageNet or very deep networks beyond ResNet-18 were not considered, similar to [34], [37], [41], [42]. TABLE II exhibits the sample size, number of object categories and numbers of training/inference samples of each dataset. The *channel* indicates red/green/blue color channel for image samples, and positive/negative spike polarity for neuromorphic spike streams. During training, we adopted the surrogate gradient function $\phi_{SG}(x) = e^{-|x|}$ for the MNIST and CIFAR-10 images, while $\phi_{SG}(x) = 1/(1+\pi^2x^2)$ for others, which have been depicted earlier in Fig. 2. Throughout our subsequent experiments, the firing thresholds and neural leakages were initialized to 1 and e^{-1} for all neurons whether they participated the synergistic learning or not, and all synaptic weights were randomly initialized following a standard Gaussian distribution (i.e., $\mu = 0$, $\sigma^2 = 1$). More simulation configurations including initial learning rates and weight decay for each case are detailed in the supplementary document.

We employed the direct input coding scheme described in Section II-B to convert pixels of image samples to spike trains. To handle the neuromorphic samples in a unified way with the direct input coding and small number of time-steps, each spike stream in the DVS-CIFAR10 and DVS-Gesture datasets were segmented into multiple slices, each of which contained the same number of successive spike events. Then, the spikes were histogrammed pixel-wisely in each slice. At every time-step t , the histogrammed spike counts in the t -th slice were fed as a pseudo-frame to the SNN [36], [44], [49]. The number of slices

TABLE II

BENCHMARK DATASETS AND SNN STRUCTURES

Dataset (sample size) ¹	N_{cat} . ²	N_{train}/N_{test} . ³	SNN	Time-steps
MNIST (1×28×28)	10	60000/10000	LeNet-5	$T = 6$
CIFAR-10 (3×32×32)	10	50000/10000	VGG-11	$T = 6$
			ResNet-18	$T = 6$
CIFAR-100 (3×32×32)	100	50000/10000	ResNet-18	$T = 6$
DVS-Gesture (2×128×128)	11	1056/288	VGG-11	$T = 20$
DVS-CIFAR10 (2×128×128)	10	9000/1000	VGG-11	$T = 10$

¹ number of channels × spatial height × spatial width.

² N_{cat} . — number of object categories.

³ N_{train} — number of training samples, N_{test} — number of testing samples.

(or equivalently, time-steps) for DVS-Gesture and DVS-CIFAR10 spike streams were set to 20 and 10, respectively.

The learning epochs were set to 200 for all datasets except MNIST, which ran only 100 epochs. Throughout all subsequent experiments unless stated otherwise, we all utilized: 1) the basic stochastic gradient descent (SGD) optimizer [54] with a momentum of 0.9, 2) a cosine annealing scheduler for learning rate [44], and 3) a batch-size of 128. All experiments were conducted on an NVIDIA RTX 3090 GPU.

Furthermore, to conduct ablation study in the effect of our synergistic learning, four variants of the STOP algorithm with different combinations of learnable parameter types were simulated to compare their learning accuracies. These variants included the basic non-synergistic rule STOP-W, the weight-threshold synergistic rule STOP-WT, the weight-leakage synergistic rule STOP-WL, and the fully synergistic rule STOP-WTL. Noticeably, for convolutional layers, all neurons in each channel share one firing threshold [46], [48]. Therefore, threshold update amounts calculated by the neurons in the same channel should be averaged before being applied to updating their shared threshold in Line 38 of Algorithm 1.

Finally, edge hardware usually prefers loss functions even simpler than the CE loss. To this end, we also evaluated SNN accuracies trained by the STOP-W and STOP-WTL rules using the computationally-light mean squared error (MSE) loss:

$$E[t] = \frac{1}{2} \sum_j \|s_j^t[t] - s_j^d\|^2 \quad (30)$$

In case of using the MSE loss, Eq. (8) should be replaced by:

$$\frac{\partial E[t]}{\partial s_j^t[t]} = s_j^t[t] - s_j^d \quad (31)$$

B. Validation Results

Fig. 4 exhibits the simulation results of our STOP algorithm with different synergistic learning policies. It reports accuracy

© 2024 IEEE. Personal use of this material is permitted. Permission from IEEE must be obtained for all other uses, in any current or future media, including reprinting/republishing this material for advertising or promotional purposes, creating new collective works, for resale or redistribution to servers or lists, or reuse of any copyrighted component of this work in other works. This work has been submitted to the IEEE for possible publication. Copyright may be transferred without notice, after which this version may no longer be accessible.

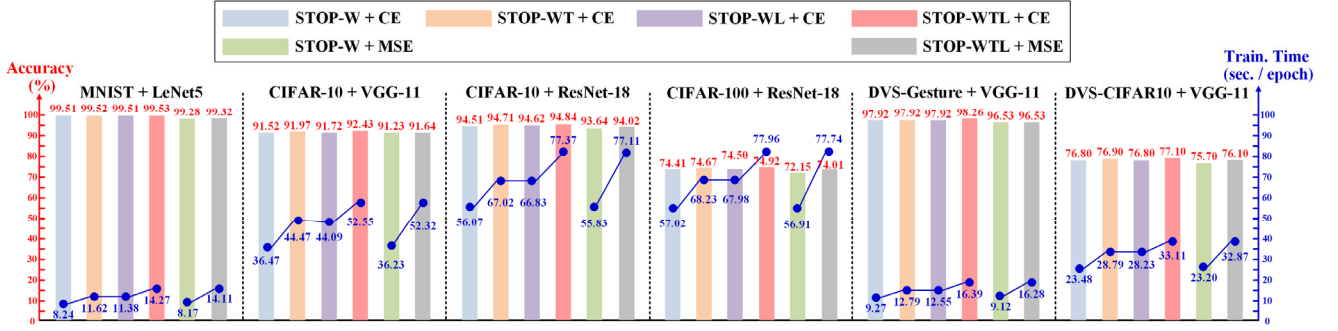


Fig. 4. Learning accuracy and latency over various datasets and SNN architectures with CE and MSE loss functions.

metrics and learning latencies across various datasets and SNN architectures with CE and MSE loss functions. Actually, we have the following key observations from two aspects.

Non-synergistic vs. synergistic learning: In Fig. 4, visual classification accuracies obtained by synergistic learning rules exceeded the accuracies attained by non-synergistic ones in almost all cases, yet at the cost of increased learning latencies. Particularly, when using the CE loss, the synergistic STOP-WT and STOP-WL achieved similar accuracies, which are higher than the non-synergistic STOP-W but lower than the fully synergistic STOP-WTL. These accuracy discrepancies between non-synergistic and fully-synergistic STOP also appeared when switching to the MSE function, as indicated in Fig. 4. Especially, the accuracy significantly increased by an amount of 1.86% from STOP-W to STOP-WTL on the challenging CIFAR-100 + ResNet-18 SNN benchmark with the MSE loss. These experimental results successfully validated the efficacy of synergistic learning for deep SNNs. However, high performance of synergistic learning comes at a cost of higher learning latencies, as shown in Fig. 4. This is in accordance with the memory complexity analysis given in Table I, as higher memory complexity implies more time consumptions on memory data accesses. The fully synergistic learning required several to around 20 more seconds than the non-synergistic baseline to accomplish one training epoch on different datasets with SNNs of varying depths. Such elongated learning time would be unacceptable in some strictly real-time or high-speed scenarios. Consequently, a careful tradeoff between accuracy performance and learning latency has to be made before a proper synergistic strategy (i.e. the non-synergistic STOP-W, the partially synergistic STOP-WT or STOP-WL, or the fully synergistic STOP-WTL) is chosen for real applications.

CE loss vs. MSE loss: When applying either non- or fully-synergistic learning to the benchmarks, the MSE loss function always behaved marginally poorly in terms of classification accuracy compared with the CE loss, exhibiting a degradation from -0.23% on the simple MNIST + LeNet-5 benchmark up to -2.26% on the more complex CIFAR-100 + ResNet-18 task using non-synergistic learning, while this gap reduced to -0.3% ~ -1.73% under the fully synergistic learning framework. On the other hand, the difference of learning latencies between using CE and MSE losses with an identical synergistic strategy

varied only on a sub-second scale when simulated in software on the GPU processor, as shown in Fig. 4. Nevertheless, when such learning procedures are required to run on customized neuromorphic hardware to enable on-chip self-adaptation, the complicated exponential and division operations in the SoftMax function to evaluate the neuronal errors in the output layer via Eq. (8) would consume a considerable amount of hardware resources [55]. So, dedicate neuromorphic hardware processors might prefer the simpler MSE loss to the CE loss unless on-chip learning accuracy is extremely pursued.

C. Work Comparison and Discussion

We have further compared the proposed STOP learning algorithm with other recently published state-of-the-art deep SNN training methods and listed their accuracy performance across common visual datasets with convolutional SNNs in Table III. Evidently, on each dataset, when using deep SNNs of similar structures and roughly the same count of time-steps, our STOP algorithm, especially the fully synergistic STOP-WTL variants, outperforms most of prior spatiotemporal gradient-based training methods. A few exceptions include the partially synergistic learning methods STL-SNN [47] and PLIF [49] conducted on the MNIST dataset. Their accuracies are marginally (0.1%~0.2%) higher than this work. The main reason might be that the MNIST images are relatively simple to reflect the actual power of distinct algorithms, and that the channel counts in the convolutional layers and the neuron counts in the FC layers of their employed SNNs far exceed those of the standard LeNet-5 structure (8C3-P2-16C3-P2-120-84- N_{cat} , where N_{cat} represents number of object categories) used by our work. It is noteworthy that the SLTT algorithm in [44] leverages an additional step called weight standardization (i.e., Gaussian normalization to $\mu = 0$ and $\sigma^2 = 1$) to improve accuracy at the cost of higher computational overheads. Although it slightly beats ours on the DVS-CIFAR10 dataset in terms of classification accuracy with the VGG-11 structure (64C3-P2-128C3-P2-256C3-256C3-P2-512C3-512C3-P2-512C3-512C3-P2-4096-4096- N_{cat}), it lags behind our metrics on all other datasets (i.e. CIFAR-10, CIFAR-100, DVS-Gesture) that they have reported accuracies on, using either VGG-11 or Resnet-18 SNN. The prefix NF- in their network names just indicates the

© 2024 IEEE. Personal use of this material is permitted. Permission from IEEE must be obtained for all other uses, in any current or future media, including reprinting/republishing this material for advertising or promotional purposes, creating new collective works, for resale or redistribution to servers or lists, or reuse of any copyrighted component of this work in other works. This work has been submitted to the IEEE for possible publication. Copyright may be transferred without notice, after which this version may no longer be accessible.

TABLE III
RELATED WORK COMPARISONS IN TERMS OF OBJECT RECOGNITION ACCURACIES.

Dataset	Method	SNN Network Architecture	Time-steps	Synergistic Learning	Accuracy (%)
MNIST	ELL [41]	12C5-P2-64C5- P2-10	$T = 10$	No (-W)	99.41%
	BELL [41]				99.40%
	FELL [41]				99.38%
	STL-SNN [47]	128C5-P2-128C5-P2-2048-10	$T = 4$	-WT	99.63%
	PLIF [49]	128C3-P2-128C3-P2-2048-100-10	$T = 8$	-WL	99.72%
	STBP [34]	LeNet-5	$T = 6$	No (-W)	98.83%
	STOP-W (ours)	LeNet-5	$T = 6$	No (-W)	99.51%
STOP-WTL (ours)	LeNet-5	$T = 6$	-WTL	99.53%	
CIFAR-10	EIHL [57]	VGG-11	$T = 6$	No (-W)	85.75%
	STOP-W (ours)	VGG-11	$T = 6$	No (-W)	91.52%
	STOP-WTL (ours)	VGG-11	$T = 6$	-WTL	92.43%
	STBP + NeuNorm [35]	CIFARNet ¹	$T = 8$	No (-W)	90.53%
	Improved STBP [46]	CIFARNet ¹	$T = 8$	-WT	89.40%
	STOP-W (ours)	CIFARNet¹	$T = 5$	No (-W)	91.75%
	STOP-WTL (ours)	CIFARNet¹	$T = 5$	-WTL	92.34%
	ELL [41]	Net2 ²	$T = 10$	No (-W)	89.40%
	BELL [41]				88.01%
	FELL [41]				88.36%
	STL-SNN [47]	Net2 ²	$T = 8$	-WT	92.42%
	PLIF [49]	Net2 ²	$T = 8$	-WL	93.50%
	STOP-W (ours)	Net2²	$T = 8$	No (-W)	93.55%
	STOP-WTL (ours)	Net2²	$T = 8$	-WTL	93.87%
	STBP + tdBN [36]	ResNet-19 ³	$T = 6$	No (-W)	93.16%
	TET [38]	ResNet-19 ³	$T = 6$	No (-W)	94.50%
	SLTT [44]	NF-ResNet-18 ⁴	$T = 6$	No (-W)	94.44%
	EIHL [57]	ResNet-18	$T = 6$	No (-W)	90.25%
	STOP-W (ours)	ResNet-18	$T = 6$	No (-W)	94.51%
	STOP-WTL (ours)	ResNet-18	$T = 6$	-WTL	94.84%
CIFAR-100	TET [38]	ResNet-19 ³	$T = 6$	No (-W)	74.72%
	SLTT [44]	NF-ResNet-18 ⁴	$T = 6$	No (-W)	74.38%
	EIHL [57]	ResNet-18	$T = 6$	No (-W)	58.63%
	STL-SNN [47]	ResNet-18	$T = 4$	-WT	72.87%
	STOP-W (ours)	ResNet-18	$T = 6$	No (-W)	74.41%
STOP-WTL (ours)	ResNet-18	$T = 6$	-WTL	74.92%	
DVS-Gesture	STL-SNN [47]	128C7-P2-128C3-P2-128C3-P2-128C3-P2-512-11	$T = 20$	-WT	97.22%
	STBP + tdBN [36]	ResNet-17 ⁵	$T = 40$	No (-W)	96.87%
	SLTT [44]	NF-VGG-11 ⁴	$T = 20$	No (-W)	97.92%
	PLIF [49]	VGG-11	$T = 20$	-WL	97.57%
	STOP-W (ours)	VGG-11	$T = 20$	No (-W)	97.92%
STOP-WTL (ours)	VGG-11	$T = 20$	-WTL	98.26%	
DVS-CIFAR10	STBP + NeuNorm [35]	128C3-128C3-P2-384C3-384C3-P2-1024-512-10	$T = 10$	No (-W)	60.50%
	STL-SNN [47]	128C7-P2-128C3-P2-128C3-P2-128C3-P2-1024-1024-10	$T = 20$	-WT	77.30%
	EIHL [57]	ResNet-18	$T = 6$	No (-W)	62.90%
	STBP + tdBN [36]	ResNet-19 ³	$T = 10$	No (-W)	67.80%
	SLTT [44]	NF-VGG-11 ⁴	$T = 10$	No (-W)	77.17%
	EIHL [57]	VGG-11	$T = 6$	No (-W)	62.45%
	PLIF [49]	VGG-11	$T = 20$	-WL	74.80%
	TET [38]	VGG-11	$T = 10$	No (-W)	76.30%
	STOP-W (ours)	VGG-11	$T = 10$	No (-W)	76.80%
STOP-WTL (ours)	VGG-11	$T = 10$	-WTL	77.10%	

¹ CIFARNet: 128C3-256C3-P2-512C3-P2-1024C3-512C3-1024-512-10.

² Net2: 256C3-256C3-256C3-P2-256C3-256C3-256C3-P2-2048-100-10

³ ResNet-19: ResNet-18 extended with one extra FC layer

⁴ NF means using weight standardization

⁵ ResNet-17: ResNet-18 with the first FC layer removed

weight standardization manipulations and does not imply structural modification [56]. Interestingly, it can be found in Table III that on the CIFAR-10 dataset, the VGG-11 SNN obtains accuracies inferior to that of the CIFARNet and Net2

structures with 2-3 less layers. We deduce this may attributed to the fact that the deeper VGG-11 requires as more as 5 pooling layers, and this leads to a total collapse of spatial information on the low-resolution 32×32 CIFAR-10 images before entering FC layers for classification. In contrast, the CIFARNet and

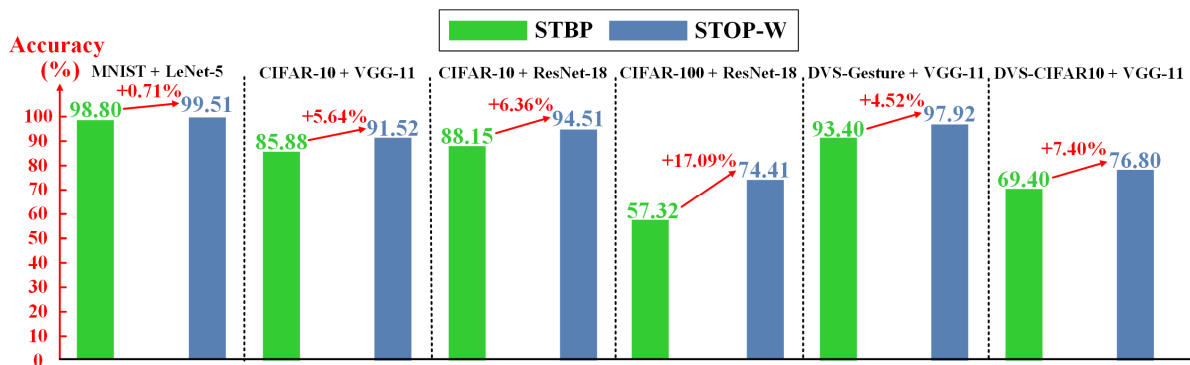


Fig. 5. Deep SNN learning accuracy comparison between the vanilla STBP algorithm [34] and the proposed STOP algorithm.

Net2 SNNs have only 2 pooling layers, thus preserving sufficient 8×8 spatial clues to facilitate better classification results in the FC layers. However, if proper deep structures are employed, such as the Resnet-18 which has a much deeper depth with residual connections, the CIFAR-10 recognition accuracy can be greatly improved, as shown in Table III. On the other side, it is observed in Table III that the works of [57] and [36] using the powerful ResNet structures obtain much lower accuracies than those employing the VGG-11 on the DVS-CIFAR10 set. The reason lies in their adopted different training/testing set partition manners. Particularly, the works in [36] and [57] have used only 8000 samples for training and left 2000 samples for testing, while other researches have taken 9000 samples for training and left just 1000 samples for testing. Consequently, the works [36] and [57] suffer a lower accuracy on the DVS-CIFAR10 due to fewer training samples. Such lack of training samples could not be compensated by the ResNet structures, or possibly even incurs overfitting issues and further degrades the accuracy when using complicated SNNs.

We have argued earlier in Section II-A that the temporal propagation of illusory spatial gradient components introduced by SG functions (as done in the STBP algorithm and its variants) would be ineffective or even detrimental to the final accuracy, and we have removed those components from our trace-based STOP framework. For a fair consolidation of such hypothesis with suppressing interference from other less relevant factors, we re-implemented the baseline STBP method [34] in PyTorch to evaluate its learning accuracy on MNIST images and other more challenging datasets under totally the same settings as we configured in Section IV-A. Fig. 5 clearly illustrates that our non-synergistic STOP-W rule significantly outperforms the basic STOP in terms of learning accuracy across all benchmarks. In Table III, the ELL [41], FELL [41] and SLTT [44] algorithms are also computed in a temporal-forward manner without propagating the illusory SG gradients during learning, yet fail to perform synergistic learning on firing thresholds or leakage parameters to further boost their recognition accuracies. On the other hand, although the works [46], [47], [49] in Table III achieve partially synergistic learning, they do not preclude the illusory components during their temporal backpropagation and their accuracies are not maximized. In comparison, to the

best of our knowledge, our STOP framework is the first one that manages to combine advantages from both temporally-forward learning procedure and synergistic learning paradigm, leading to high accuracies on challenging benchmarks without any aid of complicated optimization techniques. Our STOP framework allows a flexible choice from non- to fully-synergistic learning for deep SNNs, and thus enables tradeoffs among hardware cost and recognition accuracy upon practical demands. These characteristics make our work very attractive for resource-constrained edge intelligent applications.

V. CONCLUSION

This work proposes the STOP algorithm for high-accuracy low-memory-complexity training of deep SNNs. To achieve this goal, our algorithm enables fully weight-threshold-leakage synergistic learning under a unified temporally-forward trace-based learning framework. The employment of these temporal traces eliminates a huge memory requirement for storing neuronal states at every time-step in the forward pass, while the synergistic learning can automatically find optimal firing thresholds and leakage parameters to improve SNN accuracy. Moreover, in our STOP framework, the spatial gradients (i.e., errors) and the temporal gradients (i.e., traces) propagate orthogonally to and independently of each other, thus substantially reducing computational overheads. Elaborate experiments and work comparisons demonstrate the efficacy of the proposed algorithm across a variety of visual benchmarks and deep SNN structures. These results indicate that our method is quite suitable for self-adaptive neuromorphic intelligence at the edge with limited resources.

REFERENCES

- [1] Y. Bengio, I. Goodfellow, and A. Courville, "Deep learning," *Nature*, vol. 521, no. 7553, pp. 436–444, May 2015.
- [2] V. Sze, Y.-H. Chen, T.-J. Yang, and J. S. Emer, "Efficient Processing of Deep Neural Networks: A Tutorial and Survey," *Proceedings of the IEEE*, vol. 105, no. 12, pp. 2295–2329, Dec. 2017.
- [3] Y.-G. Ham, J.-H. Kim, and J.-J. Luo, "Deep learning for multi-year ENSO forecasts," *Nature*, vol. 573, no. 7775, pp. 568–572, Sep. 2019.
- [4] M. M. H. Shuvo, S. K. Islam, J. Cheng and B. I. Morshed, "Efficient Acceleration of Deep Learning Inference on Resource-Constrained Edge

© 2024 IEEE. Personal use of this material is permitted. Permission from IEEE must be obtained for all other uses, in any current or future media, including reprinting/republishing this material for advertising or promotional purposes, creating new collective works, for resale or redistribution to servers or lists, or reuse of any copyrighted component of this work in other works. This work has been submitted to the IEEE for possible publication. Copyright may be transferred without notice, after which this version may no longer be accessible.

- Devices: A Review," *Proceedings of the IEEE*, vol. 111, no. 1, pp. 42-91, Jan. 2023.
- [5] A. Mehonic and A. J. Kenyon, "Brain-inspired computing needs a master plan," *Nature*, vol. 604, no. 7905, pp. 255-260, Apr. 2022.
- [6] G. Li, L. Deng, H. Tang, *et al.*, "Brain-Inspired Computing: A Systematic Survey and Future Trends," *Proceedings of the IEEE*, 2024, early access, doi: 10.1109/JPROC.2024.3429360.
- [7] C. Frenkel, D. Bol and G. Indiveri, "Bottom-Up and Top-Down Approaches for the Design of Neuromorphic Processing Systems: Tradeoffs and Synergies Between Natural and Artificial Intelligence," *Proceedings of the IEEE*, vol. 111, no. 6, pp. 623-652, June 2023.
- [8] P. A. Merolla, J. V. Arthur, R. Alvarez-Icaza, *et al.*, "A million spiking-neuron integrated circuit with a scalable communication network and interface," *Science*, vol. 345, no. 6197, pp. 668-673, Aug. 2014.
- [9] M. Davies, N. Srinivasa, T.-H. Lin, *et al.*, "Loihi: a neuromorphic manycore processor with on-chip learning," *IEEE Micro*, vol. 38, no. 1, pp. 82-99, Jan. 2018.
- [10] J. Pei, L. Deng, S. Song, *et al.*, "Towards artificial general intelligence with hybrid Tianji chip architecture," *Nature*, vol. 572, no. 7767, pp. 106-111, Jul. 2019.
- [11] P. -Y. Tan and C. -W. Wu, "A 40-nm 1.89-pJ/SOP Scalable Convolutional Spiking Neural Network Learning Core With On-Chip Spatiotemporal Back-Propagation," *IEEE Trans. Very Large Scale Integration (VLSI) Systems*, vol. 31, no. 12, pp. 1994-2007, Dec. 2023.
- [12] M. Yao, O. Richter, G. Zhao, *et al.*, "Spike-based dynamic computing with asynchronous sensing-computing neuromorphic chip," *Nature Communications*, vol. 15, no. 1, pp. 1-18, May 2024.
- [13] M. De, X. Jin, S. Sun, *et al.*, "Darwin3: A large-scale neuromorphic chip with a Novel ISA and On-Chip Learning," *National Science Review*, vol. 11, no. 4, pp. 1-17, Mar. 2024.
- [14] X. Yang, C. Yao, L. Kang, *et al.*, "A Bio-Inspired Spiking Vision Chip Based on SPAD Imaging and Direct Spike Computing for Versatile Edge Vision," *IEEE Journal of Solid-State Circuits*, vol. 59, no. 6, pp. 1883-1898, Jun. 2024.
- [15] J. Zhang, D. Huo, J. Zhang, *et al.*, "ANP-I: A 28-nm 1.5-pJ/SOP Asynchronous Spiking Neural Network Processor Enabling Sub-0.1 μ J/Sample On-Chip Learning for Edge-AI Applications," *IEEE Journal of Solid-State Circuits*, vol. 59, no. 8, pp. 1-13, Aug. 2024.
- [16] M. Yin, X. Cui, F. Wei, *et al.*, "A reconfigurable FPGA-based spiking neural network accelerator," *Microelectronics Journal*, vol. 12, pp. 1-11, Oct. 2024.
- [17] T. Wang, M. Tian, H. Wang, *et al.*, "MorphBungee: A 65-nm 7.2-mm² 27- μ J/image Digital Edge Neuromorphic Chip with On-Chip 802-frame/s Multi-Layer Spiking Neural Network Learning," *IEEE Transactions on Biomedical Circuits and Systems*, 2024, early access, doi: 10.1109/TBCAS.2024.3412908.
- [18] S. R. Kheradpisheh, M. Ganjtabesh, S. J. Thorpe and T. Masquelier, "STDP-based spiking deep convolutional neural networks for object recognition," *Neural Networks*, vol. 99, pp. 56-67, Mar. 2018.
- [19] T. Zhang, X. Cheng, S. Jia, M.-M. Poo, Y. Zeng, and B. Xu, "Self-backpropagation of synaptic modifications elevates the efficiency of spiking and artificial neural networks," *Science Advances*, vol. 7, no. 43, pp. 1-11, Oct. 2021.
- [20] M. Mozafari, S. R. Kheradpisheh, T. Masquelier, A. Nowzari-Dalini and M. Ganjtabesh, "First-Spike-Based Visual Categorization Using Reward-Modulated STDP," *IEEE Transactions on Neural Networks and Learning Systems*, vol. 29, no. 12, pp. 6178-6190, Dec. 2018.
- [21] Y. Lecun, L. Bottou, Y. Bengio, and P. Haffner, "Gradient-based learning applied to document recognition," *Proceedings of the IEEE*, vol. 86, no. 11, pp. 2278-2324, Jan. 1998.
- [22] P. U. Diehl, D. Neil, J. Binas, *et al.*, "Fast-classifying, high-accuracy spiking deep networks through weight and threshold balancing," in *2015 International Joint Conference on Neural Networks (IJCNN)*, Killarney, Ireland, pp. 1-8, Jul. 2015.
- [23] B. Rueckauer, I.-A. Lungu, Y. Hu, M. Pfeiffer and S.-C. Liu, "Conversion of Continuous-Valued Deep Networks to Efficient Event-Driven Networks for Image Classification," *Frontiers in Neuroscience*, vol. 11, pp. 1-12, Dec. 2017.
- [24] B. Han, G. Srinivasan and K. Roy, "RMP-SNN: Residual Membrane Potential Neuron for Enabling Deeper High-Accuracy and Low-Latency Spiking Neural Network," *2020 IEEE/CVF Conference on Computer Vision and Pattern Recognition (CVPR)*, Seattle, WA, USA, pp. 13555-13564, Jun. 2020.
- [25] C. Stöckl and W. Maass, "Optimized spiking neurons can classify images with high accuracy through temporal coding with two spikes," *Nature Machine Intelligence*, vol. 3, no. 3, pp. 230-238, Mar. 2021.
- [26] H. Gao, J. He, H. Wang, *et al.*, "High-accuracy deep ANN-to-SNN conversion using quantization-aware training framework and calcium-gated bipolar leaky integrate and fire neuron," *Frontiers in Neuroscience*, vol. 17, pp.1-11, Mar. 2023.
- [27] Y. Guo, W. Peng, Y. Chen, *et al.*, "Joint A-SNN: Joint training of artificial and spiking neural networks via self-Distillation and weight factorization," *Pattern Recognition*, vol. 142, pp. 1-8, Oct. 2023.
- [28] Y. Hu, Q. Zheng, X. Jiang and G. Pan, "Fast-SNN: Fast Spiking Neural Network by Converting Quantized ANN," *IEEE Trans. Pattern Analysis and Machine Intelligence*, vol. 45, no. 12, pp. 14546-14562, Dec. 2023.
- [29] M. Dampfhofer, *et al.*, "Backpropagation-based learning techniques for deep spiking neural networks: A survey," *IEEE Trans. Neural Networks and Learning Systems*, vol. 35, no. 9, pp. 11906-11921, Sep. 2024.
- [30] J. K. Eshraghian, M. Ward, E. O. Neftci, *et al.*, "Training Spiking Neural Networks Using Lessons From Deep Learning," *Proceedings of the IEEE*, vol. 111, no. 9, pp. 1016-1054, Sep. 2023.
- [31] E. O. Neftci, H. Mostafa and F. Zenke, "Surrogate Gradient Learning in Spiking Neural Networks: Bringing the Power of Gradient-Based Optimization to Spiking Neural Networks," *IEEE Signal Processing Magazine*, vol. 36, no. 6, pp. 51-63, Nov. 2019.
- [32] P. J. Werbos, "Backpropagation through time: What it does and how to do it," *Proceedings of the IEEE*, vol. 78, no. 10, pp. 1550-1560, Oct. 1990.
- [33] F. Zenke and E. O. Neftci, "Brain-Inspired Learning on Neuromorphic Substrates," *Proceedings of the IEEE*, vol. 109, no. 5, pp. 935-950, May 2021.
- [34] Y. Wu, L. Deng, G. Li, J. Zhu and L. Shi, "Spatio-Temporal Backpropagation for Training High-Performance Spiking Neural Networks," *Frontiers in Neuroscience*, vol. 12, pp.1-12, May 2018.
- [35] Y. Wu, L. Deng, G. Li, J. Zhu, Y. Xie, and L. Shi, "Direct Training for Spiking Neural Networks: Faster, Larger, Better," *Proceedings of the AAAI Conference on Artificial Intelligence*, vol. 33, no. 1, pp. 1311-1318, Jul. 2019.
- [36] H. Zheng, Y. Wu, L. Deng, Y. Hu and G. Li, "Going Deeper With Directly-Trained Larger Spiking Neural Networks," *Proceedings of the AAAI Conference on Artificial Intelligence*, vol. 35, no. 12, pp. 11062-11070, May 2021.
- [37] B. Yin, F. Corradi, and S. M. Bohtë, "Accurate and efficient time-domain classification with adaptive spiking recurrent neural networks," *Nature Machine Intelligence*, vol. 3, no. 10, pp. 905-913, Oct. 2021.
- [38] S. Deng, Y. Li, S. Zhang and S. Gu, "Temporal efficient training of spiking neural network via gradient re-weighting," in *International Conference on Learning Representations (ICLR)*, pp. 1-15, Apr. 2022.
- [39] W. Fang, Y. Chen, J. Ding, *et al.*, "SpikingJelly: An open-source machine learning infrastructure platform for spike-based intelligence," *Science Advances*, vol. 9, no. 40, pp. 1-18, Oct. 2023.
- [40] G. Bellec, F. Scherr, A. Subramoney, *et al.*, "A solution to the learning dilemma for recurrent networks of spiking neurons," *Nature Communications*, vol. 11, no. 1, pp. 1-15, Jul. 2020.
- [41] C. Ma, R. Yan, Z. Yu, and Q. Yu, "Deep Spike Learning With Local Classifiers," *IEEE Trans. Cybernetics*, vol. 53, no. 5, pp. 3363-3375, May 2023.
- [42] T. Bohnstingl, S. Woźniak, A. Pantazi, and E. Eleftheriou, "Online Spatio-Temporal Learning in Deep Neural Networks," *IEEE Trans. Neural Networks and Learning Systems*, vol. 34, no. 11, pp. 8894-8908, Nov. 2023.
- [43] B. Yin, F. Corradi, and S. M. Bohtë, "Accurate online training of dynamical spiking neural networks through Forward Propagation Through Time," *Nature Machine Intelligence*, vol. 5, no. 5, pp. 518-527, May 2023.
- [44] Q. Meng, M. Xiao, S. Yan, *et al.*, "Towards Memory- and Time-Efficient Backpropagation for Training Spiking Neural Networks," *2023 IEEE/CVF International Conference on Computer Vision (ICCV)*, Paris, France, pp. 6143-6153, Oct. 2023.
- [45] R. Xiao, L. Ning, Y. Wang, H. Du, S. Wang, and R. Yan, "Asymmetric Spatio-Temporal Online Learning for Deep Spiking Neural Networks," *IEEE Transactions on Cognitive and Developmental Systems*, 2024, early access, doi: 10.1109/TCDS.2023.3278720.
- [46] P. -Y. Tan, C. -W. Wu and J. -M. Lu, "An Improved STBP for Training High-Accuracy and Low-Spike-Count Spiking Neural Network," *2021 Design, Automation & Test in Europe Conference & Exhibition (DATE)*, Grenoble, France, pp. 575-580, Feb. 2021.

© 2024 IEEE. Personal use of this material is permitted. Permission from IEEE must be obtained for all other uses, in any current or future media, including reprinting/republishing this material for advertising or promotional purposes, creating new collective works, for resale or redistribution to servers or lists, or reuse of any copyrighted component of this work in other works. This work has been submitted to the IEEE for possible publication. Copyright may be transferred without notice, after which this version may no longer be accessible.

- [47] H. Sun, W. Cai, B. Yang, Y. Cui, Y. Xia, D. Yao, and D. Guo, "A Synapse-Threshold Synergistic Learning Approach for Spiking Neural Networks," *IEEE Transactions on Cognitive and Developmental Systems*, vol. 16, no. 2, pp. 544–558, Apr. 2024.
- [48] N. Rathi and K. Roy, "DIET-SNN: A Low-Latency Spiking Neural Network With Direct Input Encoding and Leakage and Threshold Optimization," *IEEE Transactions on Neural Networks and Learning Systems*, vol. 34, no. 6, pp. 3174–3182, Jun. 2023.
- [49] W. Fang, Z. Yu, Y. Chen, *et al.*, "Incorporating Learnable Membrane Time Constant to Enhance Learning of Spiking Neural Networks," *2021 IEEE/CVF International Conference on Computer Vision (ICCV)*, Montreal, QC, Canada, pp. 2661–2671, Oct. 2021.
- [50] F. Li, D. Li, C. Wang, *et al.*, "An artificial visual neuron with multiplexed rate and time-to-first-spike coding," *Nature Communications*, vol. 15, no. 3689, May 2024.
- [51] A. Krizhevsky, "Learning multiple layers of features from tiny images," Dept. Comput. Sci., Univ. Toronto, Toronto, ON, USA, Rep. TR-2009, 2009. [Online]. Available: <http://www.cs.toronto.edu/~kriz/learningfeatures-2009-TR.pdf>
- [52] A. Amir, B. Taba, D. Berg, *et al.*, "A low power, fully event-based gesture recognition system," *2017 IEEE Conference on Computer Vision and Pattern Recognition (CVPR)*, Honolulu, HI, USA, pp. 7388–7397, Jul. 2017.
- [53] H. Li, H. Liu, X. Ji, G. Li, and L. Shi, "CIFAR10-DVS: an event-stream dataset for object classification," *Frontiers in neuroscience*, vol. 11, pp. 1–10, Jun. 2017.
- [54] I. Loshchilov and F. Hutter, "SGDR: Stochastic gradient descent with warm restarts," In *International Conference on Learning Representations (ICLR)*, Palais des Congrès Neptune, Toulon, France, pp. 1–16, Apr. 2017.
- [55] J. Kim, S. Kim, K. Choi and I. -C. Park, "Hardware-Efficient SoftMax Architecture With Bit-Wise Exponentiation and Reciprocal Calculation," *IEEE Transactions on Circuits and Systems I: Regular Papers*, vol. 71, no. 10, pp. 4574–4585, Oct. 2024.
- [56] A. Brock, S. De, S. L. Smith, K. Simonyan, "High-Performance Large-Scale Image Recognition Without Normalization," *Proceedings of the 38th International Conference on Machine Learning (ICML)*, pp.1059–1071, Jul. 2021.
- [57] T. Jiang, Q. Xu, X. Ran, *et al.*, "Adaptive deep spiking neural network with global-local learning via balanced excitatory and inhibitory mechanism," in *International Conference on Learning Representations (ICLR)*, pp. 1–12, Vienna, Austria, Jan. 2024.

Haoran Gao (S'21) received the B.S. degree in electronic information engineering from Nanjing University of Information Science and Technology, Nanjing, China, in June 2021. He is currently working toward the Ph.D. degree with the School of Microelectronics and Communication Engineering, Chongqing University, Chongqing, China. His research interests include neuromorphic computing algorithms.

Xichuan Zhou (S'06–M'13–SM'21) received the B.S. and Ph.D. degrees from Zhejiang University, Hangzhou, China, in 2005 and 2010, respectively. He was a Visiting Scholar with Arizona State University, Tempe, AZ, USA, in 2009. He was the Vice Dean of the School of Microelectronics and Communication Engineering, Chongqing University, in 2022. He is currently the Director of the Institute of Science on Brain Inspired Intelligence, Chongqing University, Chongqing, China. He made original contributions to intelligent edge computing, significantly contributing to both efficient deep learning methods and engineering applications. He has authored or coauthored more than 60 papers in prestigious international

journals and conferences, including IEEE TNNLS, IEEE TCAS-I, IEEE TED, IEEE TBioCAS, IEEE SPL, IEEE GRSL, ICML, AAAI, and CVPR. His monograph of Deep Learning on Edge Computing Devices is one of the earliest books covering multidisciplinary topics from algorithm to hardware design of embedded AI systems. He also held over a dozen patents and has given numerous keynote speeches and invited talks, and chaired several conferences. He was awarded the Outstanding Scientist of Chinese Institute of Electronics in 2021.

Yingcheng Lin received his B.S. M.S. and Ph.D. degrees in electrical engineering from Chongqing University, Chongqing, China, in 2006, 2009 and 2014, respectively. Since 2017, he is an associate professor with the School of Microelectronics and Communication Engineering, Chongqing University, China. He is engaged in high-performance embedded signal processing system designs.

Min Tian (M'17) received her B.S. degree from Sun-Yat Sen University, Guangzhou, China, in 2014, and the Ph.D. degree from the Institute of Microelectronics, Chinese Academy of Sciences, Beijing, China, in 2019. From Oct. 2020 to Aug. 2023, she was a research assistant professor with the School of Microelectronics and Communication Engineering, Chongqing University, Chongqing, China, where she has been a lecturer from Sept. 2023 to Aug. 2024. She is currently a senior engineer with Chongqing United Microelectronics Center Co. Ltd, Chongqing, China. Her research interests include emerging semiconductor technology, devices and circuits for ubiquitous AIoT applications.

Liyuan Liu (M'11) received the B.S. and Ph.D. degrees in Electrical Engineering from the Electronic Engineering Department, Institute of Microelectronics, Tsinghua University, China, in 2005 and 2010, respectively. He is currently a full professor with the Institute of Semiconductors, Chinese Academy of Sciences, Beijing, China. His research interests include high-end AI-enabled vision sensors, processors and algorithms.

Cong Shi (S'13–M'17) received his B.S. degree in electronic information science and technology, M.S. degree in microelectronics from Harbin Institute of Technology, Harbin, China, in 2007 and 2009, respectively, and the Ph.D. degree in electrical engineering from Tsinghua University, Beijing, China, in 2014. He was also a joint Ph.D. student at the Institute of Semiconductors, Chinese Academy of Sciences, Beijing, China. From 2015 to 2018, he was a postdoctoral fellow with the Schepens Eye Research Institute, Massachusetts Eye and Ear, Harvard Medical School, Boston, MA. He is currently a research professor with the School of Microelectronics and Communication Engineering, Chongqing University, Chongqing China, where he leads a research group in AI chip designs for smart visual processing and neuromorphic systems

Supplementary Materials

S1. EXPERIMENTAL SETTINGS

A. Dataset and Network Configurations

Table S1. Detailed learning configurations used in our experiments.

Dataset	SNN	Time-steps	Synergistic Strategy	Loss	Initial Learning Rate*	Weight Decay
MNIST	LeNet-5	$T = 6$	STOP-W	CE	$\eta_w = 5 \times 10^{-4}$	0
			STOP-WT		$\eta_w = 5 \times 10^{-4}$ $\eta_\theta = 5 \times 10^{-5}$	
			STOP-WL		$\eta_w = 5 \times 10^{-4}$ $\eta_a = 5 \times 10^{-5}$	
			STOP-WTL		$\eta_w = 5 \times 10^{-4}$ $\eta_\theta = 4 \times 10^{-5}$ $\eta_a = 4 \times 10^{-5}$	
			STOP-W	MSE	$\eta_w = 5 \times 10^{-4}$	
			STOP-WTL		$\eta_w = 5 \times 10^{-4}$ $\eta_\theta = 4 \times 10^{-5}$ $\eta_a = 4 \times 10^{-5}$	
CIFAR-10	VGG-11	$T = 6$	STOP-W	CE	$\eta_w = 1 \times 10^{-2}$	1×10^{-5}
			STOP-WT		$\eta_w = 1 \times 10^{-2}$ $\eta_\theta = 2 \times 10^{-4}$	
			STOP-WL		$\eta_w = 1 \times 10^{-2}$ $\eta_a = 2 \times 10^{-4}$	
			STOP-WTL		$\eta_w = 1 \times 10^{-2}$ $\eta_\theta = 1 \times 10^{-4}$ $\eta_a = 1 \times 10^{-4}$	
			STOP-W	MSE	$\eta_w = 1 \times 10^{-2}$	
	STOP-WTL	$\eta_w = 1 \times 10^{-2}$ $\eta_\theta = 1 \times 10^{-4}$ $\eta_a = 1 \times 10^{-4}$				
	ResNet-18	$T = 6$	STOP-W	CE	$\eta_w = 1 \times 10^{-1}$	3×10^{-4}
			STOP-WT		$\eta_w = 1 \times 10^{-1}$ $\eta_\theta = 5 \times 10^{-4}$	
			STOP-WL		$\eta_w = 1 \times 10^{-1}$ $\eta_a = 3 \times 10^{-4}$	
			STOP-WTL		$\eta_w = 1 \times 10^{-1}$ $\eta_\theta = 3 \times 10^{-4}$ $\eta_a = 1 \times 10^{-4}$	
STOP-W			MSE	$\eta_w = 1 \times 10^{-1}$		
STOP-WTL	$\eta_w = 1 \times 10^{-1}$ $\eta_\theta = 3 \times 10^{-4}$ $\eta_a = 1 \times 10^{-4}$					
CIFAR-100	ResNet-18	$T = 6$	STOP-W	CE	$\eta_w = 1 \times 10^{-1}$	5×10^{-4}
			STOP-WT		$\eta_w = 1 \times 10^{-1}$ $\eta_\theta = 1 \times 10^{-3}$	
			STOP-WL		$\eta_w = 1 \times 10^{-1}$ $\eta_a = 1 \times 10^{-3}$	
			STOP-WTL		$\eta_w = 1 \times 10^{-1}$ $\eta_\theta = 5 \times 10^{-4}$ $\eta_a = 5 \times 10^{-4}$	
			STOP-W	MSE	$\eta_w = 1 \times 10^{-1}$	
			STOP-WTL		$\eta_w = 1 \times 10^{-1}$ $\eta_\theta = 5 \times 10^{-4}$ $\eta_a = 5 \times 10^{-4}$	

DVS-Gesture	VGG-11	$T = 20$	STOP-W	CE	$\eta_w = 1 \times 10^{-1}$	5×10^{-4}
			STOP-WT		$\eta_w = 1 \times 10^{-1}$ $\eta_\theta = 1 \times 10^{-3}$	
			STOP-WL		$\eta_w = 1 \times 10^{-1}$ $\eta_\alpha = 1 \times 10^{-3}$	
			STOP-WTL		$\eta_w = 1 \times 10^{-1}$ $\eta_\theta = 4 \times 10^{-4}$ $\eta_\alpha = 2 \times 10^{-4}$	
			STOP-W	MSE	$\eta_w = 1 \times 10^{-1}$	
			STOP-WTL		$\eta_w = 1 \times 10^{-1}$ $\eta_\theta = 4 \times 10^{-4}$ $\eta_\alpha = 2 \times 10^{-4}$	
DVS-CIFAR10	VGG-11	$T = 10$	STOP-W	CE	$\eta_w = 5 \times 10^{-2}$	5×10^{-4}
			STOP-WT		$\eta_w = 5 \times 10^{-2}$ $\eta_\theta = 4 \times 10^{-4}$	
			STOP-WL		$\eta_w = 5 \times 10^{-2}$ $\eta_\alpha = 2 \times 10^{-4}$	
			STOP-WTL		$\eta_w = 5 \times 10^{-2}$ $\eta_\theta = 3 \times 10^{-4}$ $\eta_\alpha = 1 \times 10^{-4}$	
			STOP-W	MSE	$\eta_w = 5 \times 10^{-2}$	
			STOP-WTL		$\eta_w = 5 \times 10^{-2}$ $\eta_\theta = 3 \times 10^{-4}$ $\eta_\alpha = 1 \times 10^{-4}$	

* Initial learning rate for cosine annealing.